# SIMPLE SCALAR MODEL AND ANALYSIS FOR LARGE AMPLITUDE OSCILLATORY SHEAR

DIMITRI MERGER<sup>1</sup>, MAHDI ABBASI<sup>1</sup>, JURI MERGER<sup>2</sup>, A. JEFFREY GIACOMIN<sup>3</sup>, CHAIMONGKOL SAENGOW<sup>3,4</sup>, MANFRED WILHELM<sup>1</sup>

<sup>1</sup>Institut für Technische Chemie und Polymerchemie, Karlsruher Institut für Technologie, 76128 Karlsruhe, Germany

<sup>2</sup>Institut für Mathematik, Universität Würzburg, 97074 Würzburg, Germany
<sup>3</sup>Chemical Engineering Department, Queen's University, Kingston, ON K7L 3N6, Canada
<sup>4</sup>Polymers Research Center, King Mongkut's University of Technology, North Bangkok,
Bangkok 10800, Thailand

Corresponding author: manfred.wilhelm@kit.edu

Received: 27.5.2016, Final version: 22.07.2016

#### ABSTRACT:

This work presents a simple, scalar model for predicting a nonlinear shear stress response of a viscoelastic fluid in Large Amplitude Oscillatory Shear (LAOS) experiments. The model is constructed by replacing the viscosity in the well-known Maxwell model by a shear rate dependent viscosity function. By assuming the empirical Cox-Merz rule to be valid, this shear rate dependent viscosity function is specified based on the Maxwell expression for the complex viscosity. We thus construct a particular case of the White-Metzner constitutive equation. Numerical solutions as well as an asymptotic analytical solution of the model are presented. The results, analyzed for higher harmonic content by Fourier transform, are compared to experimental data of a viscoelastic solution of wormlike micelles based on cetyltrimethylammonium bromide. Good agreement is found for low frequencies, where viscous properties dominate.

#### **KEY WORDS:**

Large Amplitude Oscillatory Shear (LAOS), constitutive modeling, Cox-Merz rule, Maxwell model, non-linear rheology, worm-like micelles

#### 1 INTRODUCTION

Nonlinear viscoelasticity plays a crucial role for the mechanical behavior of complex fluids (e.g. polymer melts, polymer solutions, and dispersions) under many processing and application conditions. The use of Large Amplitude Oscillatory Shear (LAOS) experiments, where a sample is subjected to a sinusoidal shear deformation  $\gamma(t) = \gamma_0 \sin(\omega t)$  has become a common technique to probe nonlinear viscoelasticity of materials [1-6]. Its main advantage is the possibility to investigate the effect of both characteristic dynamic variables, the Deborah number De and the Weissenberg number Wi using the same test with the most common rheological equipment, a rotational rheometer. The Deborah number  $De = \lambda/\tau_o$  is defined as the ratio of a characteristic relaxation time of a material  $\lambda$  and a characteristic time of observation  $\tau_o$ , which for oscillatory flow is the inverse of the angular frequency  $\tau_o = 1/\omega$ . This *De* measures to which degree elastic effects influence the overall mechanical response. The Weissenberg number  $Wi = \lambda/\tau_d$  is the ratio of  $\lambda$  and a characteristic time of the deformation  $\tau_d$ . For steady shear  $\tau_d$  is the inverse of the shear rate  $\tau_d = 1/\dot{\gamma}$  whereas for oscillatory shear  $\tau_d = 1/\dot{\gamma}_o = 1/(\omega\gamma_o)$  [7], where  $\dot{\gamma}_o$  denotes the shear rate amplitude. The Weissenberg number can be interpreted as a dimensionless shear rate, indicating the influence of nonlinear behavior. Further advantages of using LAOS to probe nonlinear viscoelasticity include the omission of sudden signal jumps in the strain input, as in step experiments, and the ability to probe large strain rates without edge failure [8].

Recent efforts in constitutive modeling of LAOS behavior have led to approximate solutions that provide material functions for a couple of nonlinear models. Whereas some of these are truncated expansions in the shear rate amplitude (corotational Maxwell [9]), or in the shear strain amplitude (Giesekus [10] and Pom-Pom [11]). Others are asymptotic solutions, such as the molecular stress function model [12, 13] and a thixotropic

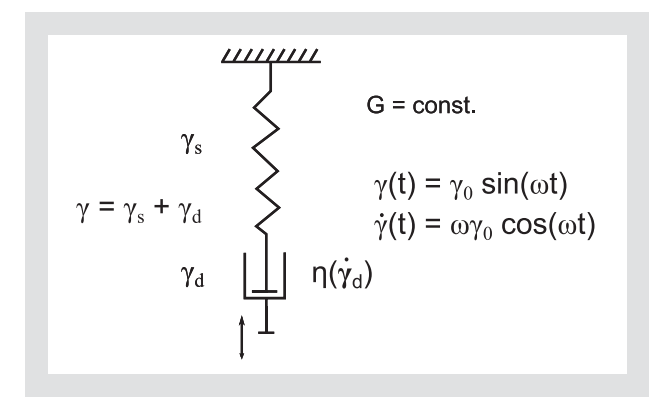


Figure 1: Phenomenological model consisting of a linear spring and a nonlinear dashpot in series. The introduction of a nonlinear dashpot is a simple way to introduce nonlinearity into the Maxwell model.

Jefferson model [8]. For the corotational Maxwell model also an exact solution [14] is available. Although analytical solutions are generally preferred because material functions can be calculated explicitly, arriving at these solutions usually involves careful tedium. In most cases, only truncated power series expanded in strain amplitude or shear rate amplitude can be obtained. Furthermore, the work needed to determine the next order, that is, to add the next harmonic, increases disproportionately. Though this work does yield the next harmonic, it can yield little improvement in the shear stress overall.

Exact analytical solutions are available for the scalar formulation of the Prandl element [15], which describes a yield stress fluid and also the tensorial corotational Maxwell model [14]. However, the discontinuities in the Prandl model limit its use for describing oscillatory shear behavior beyond yield. The corotational Maxwell model [9] might indeed be the simplest tensorial model, which can predict nonlinear shear stress response for LAOS flow. Its nonlinearity stems from the corotational derivative of the stress tensor but the tensor calculus needed to understand this model is often beyond the general knowledge of LAOS users, especially those not proficient in fluid dynamics. Additionally, the exact solution [14] is too cumbersome, as it involves two infinite series, each containing one Bessel function.

Therefore, this work presents a simple scalar, one dimensional LAOS model, with specific interest towards the storage and the loss modulus G' and G'' and the relative intensity of the third harmonic  $I_{3/1}$  with their respective strain amplitude  $\gamma_o$  and angular frequency  $\omega$  dependencies. The storage and loss moduli beyond the linear viscoelastic regime are defined based on the cosine and sine terms of the fundamental harmonic  $\sigma_1$  as  $G' = \cos \delta_1$  and  $G'' = \sin \delta_1$ . Furthermore, we focus on the intrinsic nonlinearity  $Q_o = \lim_{\gamma_o \to o} I_{3/1}/\gamma_o^2$  [16, 17], which is derived from  $I_{3/1}$  in the limit of small strain amplitudes. Several alternative frameworks to quantify nonlinear behavior in LAOS exist [6, 9, 18], including intrinsic parameters [19, 20] as well as local wave form descriptors [21, 22]. We have chosen to use the third har-

monic intensity and the intrinsic nonlinearity to diminish the number of observable parameters. We also restrict ourselves to these magnitude related measures because they can be obtained quickly and reliably, they do not depend on the strain input reference (sine or cosine) and therefore, do not require further data processing such as phase correction, which is necessary for example for analyses based on higher harmonic phases [4, 23] or Chebishev coefficients [19]. The model is intentionally scalar for simplicity, consequently only shear forces are considered and normal forces are not addressed. To construct this model, the constant viscosity of the dashpot in the common Maxwell model will be replaced by a shear rate dependent viscosity function. This results in a special case of the White-Metzner model [24].

#### 2 MODIFICATION OF THE MAXWELL MODEL

#### 2.1 DIFFERENTIAL EQUATION

Starting from the scalar Maxwell model, which is a linear combination of a Hookean spring and a Newtonian dashpot [25, 26], the simplest way to generate nonlinear behavior is to introduce only one nonlinear building block in the model. Consequently we have to replace either the spring's modulus or the dashpot's viscosity by a nonlinear function. Since the viscosity is known to be very much shear rate dependent for many complex fluids [25-27], typical changes can be of the order of one or two decades, we have chosen to describe the dashpot by a nonlinear function  $\eta(\dot{\gamma})$ . Previous work by Zacharatos and Kontou focused on modeling of strain-stress curves and start-up of steady shear behavior using a nonlinear phenomenological model based on the standard solid model (a spring parallel with a Maxwell element) [28]. They used an Eyring type nonlinear dashpot [29] as well as a nonlinear spring which followed a power law. LAOS flow, however, was not modeled. Similarly, but based on the Maxwell model, Monsia calculated stress build up for a step strain experiment with a model consisting of a generalized spring, described by a power law in strain, and generalized dashpot, described by a power law in shear rate [30]. Since our aim is to keep the model as simple as possible, nonlinearity of the spring will be not considered. Although nonlinearities in the elastic behavior are well known and can be considered by finite extensible spring models [31], we think their effect is negligible in comparison to the substantial nonlinearity in the viscous behavior.

To set up the differential equation for the serial combination of the linear spring with a nonlinear dashpot as depicted in Figure 1, the same procedure as for

the Maxwell model is used. Both elements, spring and dashpot, experience the same shear stress  $\sigma$  and the sum of the individual strains in the spring and the dashpot,  $\gamma_s$  and  $\gamma_d$ , equals the total strain  $\gamma$ . The sum of the individual shear rates equals the total shear rate.

$$\sigma_{s} = \sigma_{d} \tag{1}$$

$$\gamma = \gamma_s + \gamma_d \tag{2}$$

$$\dot{\gamma} = \dot{\gamma}_s + \dot{\gamma}_d \tag{3}$$

Assuming linear behavior of the spring  $\dot{\gamma}_s$  can be replaced by  $\dot{\sigma}'/G$  using Hooke's law, for the dashpot shear rate,  $\dot{\gamma}_d = \sigma/\eta(\dot{\gamma}_d)$  will be used. This leads to the first order ordinary differential equation (Equation 5), which is the scalar expression for the shear stress of the White-Metzner model [24]. Recently, a multimode version of this model has been successfully applied to model the nonlinear viscoelasticity of a silicone oil at Deborah numbers smaller than one [32]. In the current work, we strive for an even simpler description, test the applicability of a single mode model and also extend the investigated De number range to the elastically dominated regime (De > 1).

$$\dot{\gamma} = \frac{\dot{\sigma}}{G} + \frac{\sigma}{\eta(\dot{\gamma}_d)} \tag{4}$$

$$\dot{\sigma} = G \left( \dot{\gamma} - \frac{\sigma}{\eta(\dot{\gamma}_d)} \right) \tag{5}$$

### 2.2 CHOICE OF THE SHEAR RATE DEPENDENT VISCOSITY FUNCTION

When specifying the shear rate dependent viscosity function of a polymer, two major features are important: a finite zero shear viscosity  $\eta_o$  and the power law index of the shear thinning. Many empirical viscosity functions have been proposed which capture these two features [29], well known examples are the Carreau-Yasuda [33] and the Cross model [34]. In the here presented work, a two parameter viscosity function will be used that can be derived from the Maxwell-Model using the Cox-Merz rule [35]. This empirical rule states that for simple viscoelastic materials the angular frequency dependent complex shear viscosity in a small amplitude oscillatory test equals the shear rate dependent viscosity in a steady shear experiment  $|\eta^*(\omega)| = \eta(\dot{\gamma})$ , where  $\omega$  is expressed in units of rad/s and  $\dot{\gamma}$  in 1/s. Snijkers and

Vlassopoulos have recently reported applicability of this rule for a variety of polymer melts including linear and branched polymers as well as blends of linear polymers of the same chemistry [36]. Although the Cox-Merz rule generally lacks a physical explanation, it is applied frequently in both, academic and industrial research. Its main application is to easily determine the steady shear viscosity function from the results of small amplitude oscillatory shear (SAOS) experiments. This is advantageous because the SAOS experiment generally is more robust and more reproducible than the steady shear experiment. Once the Cox-Merz relationship has been verified for a particular system, high shear rate viscosities can be conveniently obtained from SAOS tests which avoid the sample failure and slip artifacts that usually restrict capillary rheometer experiments. Additionally, in comparison with using a capillary rheometer, less sample is needed. Furthermore, if time temperature superposition is applicable, even higher shear rates are accessible because of the increased range of angular frequencies that can be probed. Detailed discussion on the merits of this rule can be found in other references [25, 36]. In the Maxwell model, the storage and loss moduli G'and G" are frequency-dependent functions following Equation 6. The magnitude of complex shear viscosity is connected to G' and G" by Equation 7 [29]. Inserting Equation 6 into Equation 7 and simplifying yields the final expression in Equation 7. Applying the Cox-Merz rule,  $|\eta^*(\omega)|$  is replaced by  $\eta(\dot{\gamma})$  and the angular frequency dependence is changed to a shear rate dependence, which results in Equation 8.

$$G'(\omega) = G \frac{\lambda^2 \omega^2}{1 + \lambda^2 \omega^2}$$

$$G''(\omega) = G \frac{\lambda \omega}{1 + \lambda^2 \omega^2}$$
(6)

$$|\eta^{*}(\omega)| = \sqrt{\eta'^{2}(\omega) + \eta''^{2}(\omega)}$$

$$= \sqrt{(G''/\omega)^{2} + (G'/\omega)^{2}}$$

$$= G\lambda\sqrt{\left(\frac{1}{1+\lambda^{2}\omega^{2}}\right)^{2} + \left(\frac{\lambda\omega}{1+\lambda^{2}\omega^{2}}\right)^{2}}$$

$$= G\lambda\sqrt{\frac{1+\lambda^{2}\omega^{2}}{1+2\lambda^{2}\omega^{2} + \lambda^{4}\omega^{4}}}$$

$$= G\lambda\sqrt{\frac{1}{1+\lambda^{2}\omega^{2}}}$$
(7)

$$\eta(\dot{\gamma}) = G\lambda \sqrt{\frac{1}{1 + \lambda^2 \dot{\gamma}^2}} \tag{8}$$

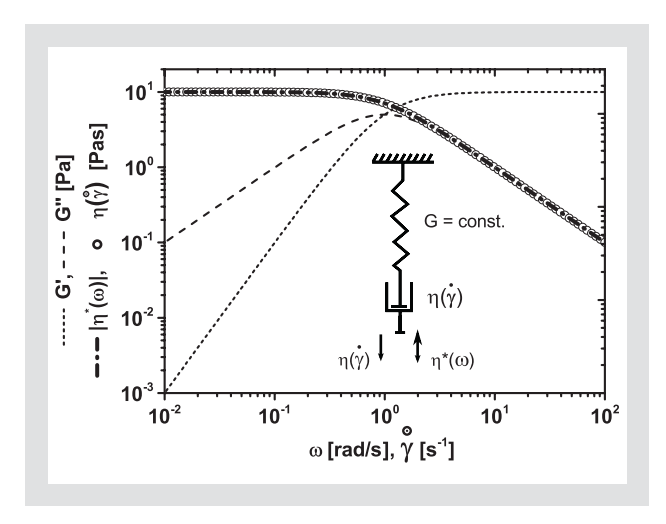


Figure 2: The frequency dependencies of the storage and loss moduli for the presented model are identical to the Maxwell model. Furthermore, in contrast to the Maxwell model, the Cox-Merz rule  $|\eta^*(\omega)| = \eta(\dot{\gamma})$  is incorporated for G = 10 Pa and  $\lambda$  = 1 S.

Thus the zero shear viscosity in Equation 8 is  $\eta_O = G\lambda$  and the square root term causes shear thinning behavior for high shear rates. The form of Equation 8 is a particular case of the Carreau model (Equation 9, [33]) with c = 0 and  $\eta_\infty = 0$ .

$$\eta(\dot{\gamma}) = \frac{\eta_o - \eta_\infty}{\left(\imath + \lambda^2 \dot{\gamma}^2\right)^{(\imath - c)/2}} + \eta_\infty \tag{9}$$

Substituting Equation 8 into Equation 5 results in a differential equation according to Equation 10. The specific choice of  $\eta(\dot{\gamma})$  keeps the number of parameters for the whole model minimal using only a single elastic modulus G and a single relaxation time  $\lambda$ .

$$\dot{\sigma} = G\dot{\gamma} - \frac{\sigma}{\lambda} \sqrt{1 + \lambda^2 \dot{\gamma}^2} \tag{10}$$

In the presented model, the relaxation time  $\lambda$  defines the balance between elastic and viscous behavior for a fixed excitation frequency and the nonlinearity in the viscosity function at the same time. The modulus G linearly varies the overall stress magnitude of the response, thus providing a scale for G' and G". In Figure 2 a plot of the storage and loss moduli as well as the steady shear and the complex viscosity functions for the modified Maxwell model (Equation 5) are shown. The classic Maxwell model predicts a constant viscosity for steady shear, whereas the complex viscosity is a function of  $\omega$ . By incorporating the Cox-Merz rule with the specific choice of the shear rate dependent viscosity (Equation 8), Maxwellian behavior for the linear oscillatory case is combined with shear thinning in steady shear. Such a modification of the Maxwell model allows one to predict nonlinear effects in steady shear and also in oscillatory shear for arbitrary strain amplitudes.

### 3 NUMERICAL AND EXPERIMENTAL METHODS

## 3.1 NUMERICAL SOLUTION OF THE DIFFERENTIAL EQUATION

The model represented by Equation 10 was solved using a custom-written code in MATLAB (version R2014a, MathWorks, 3 Apple Hill Drive, Natick, MA 01760-2098, USA), which employed a 4<sup>th</sup> order Runge-Kutta scheme [37]. For every oscillation cycle, 512 points equally spaced in time were calculated, which is a typical sampling rate in an experiment. For a set of G and  $\lambda$  the initial value problem was solved for varying strain amplitudes  $\gamma_o$  at a fixed angular frequency  $\omega$  thus varying  $Wi = \omega \gamma_o \lambda$ , while keeping  $De = \lambda \omega$  fixed. For every strain amplitude, 55 oscillation cycles were calculated from which the first 50 were discarded to eliminate the influence of start-up. Cycles 51 to 55 were Fourier-transformed using MATLAB and G', G'', and  $I_{3/1}$  were calculated from the spectra. Typical signal-to-noise ratios in the spectra were of the order of 10<sup>-8</sup> to 10<sup>-7</sup>. Weissenberg number dependent calculations were repeated for various De.

#### 3.2 EXPERIMENTAL PROCEDURES

LAOS experiments were performed on a 0.15 M aqueous solution of cetyltrimethylammonium bromide (CTAB, obtained from Sigma Aldrich), containing potassium bromide (1.5 M, obtained from Sigma Aldrich) following the recipe of Lequeux et al. [38]. At a concentration of 0.15 M, CTAB forms wormlike micelles long enough to entangle, resulting in viscoelastic behavior [10, 38, 39]. Complete dissolution of CTAB and KBr was ensured by stirring the sample at 40 °C for 48 hours. Linear frequency dependent measurements, flow curve measurements and LAOS experiments were performed using an ARES-G2 strain controlled rheometer (TA Instruments), equipped with a torsional, concentric cylinder geometry ( $r_1$  = 18.6 mm and  $r_2$  = 20 mm) and a Peltier temperature control system. The measurement temperature was T = 35 °C. For the LAOS tests, the sample was subjected to a sinusoidal excitation  $\gamma = \gamma_0 \sin(\omega t)$ . The oscillating stress signals were recorded using the commercial rheometer software TRIOS (version 3.3.0.4055, TA Instruments, 159 Lukens Drive, New Castle, DE 19720, USA). Data was analyzed using the same MATLAB code that was employed for the analysis of the numerical solutions. Repeated measurements were analyzed using the automatic Fourier transform in the TRIOS software after confirmation that both analysis routines give identical results.

In our experiments, the dominant nonlinear effect is shear thinning at high shear rates for steady shear

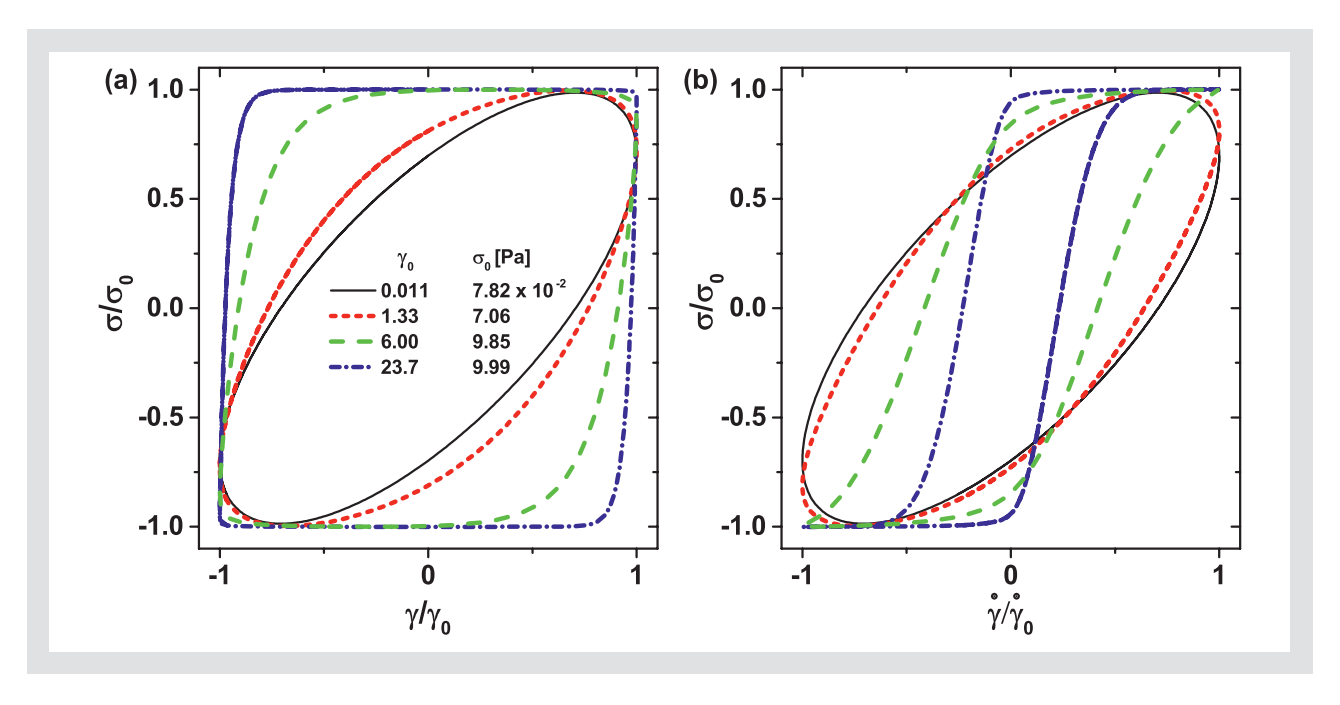


Figure 3: Waveforms from a numerical solution of the model using G = 10 Pa,  $\lambda = 1$  s,  $\omega = 1$  rad/s, De = 1, represented as elastic (a) and viscous (b) Lissajous figures.

flow and intercycle shear thinning for LAOS flow as evident in the decrease of G' and G'' (Equations 11 and 12) with increasing strain amplitude for all investigated frequencies. In addition to this sample nonlinearity, instabilities in the flow field can occur at high shear rates. Wormlike micelles systems are known to form shear bands which has been observed by NMR velocity imaging [40, 41] and light scattering techniques [42]. A commonly observed rheological signature of shear banding in WLM solutions is a stress plateau in the flow curve that can stretch over an order of magnitude in shear rate [43, 44]. Helgeson et al. [45] have observed this shear banding instability by particle imaging velocimetry and gap resolved neutron scattering for a 16.7 wt% CTAB sample at 32 °C. The banding in their sample was connected to an isotropic-nematic transition. Shear banding has also been observed for a 22 wt% CTAB solution at 32 °C in oscillatory shear [10]. Typical Wi numbers for the onset of shear banding in those studies were 0.7 [44] or 0.47 [10].

In our LAOS experiments, however, the extended stress plateau characteristic for shear banding was not observed in the measured strain amplitude range (usually 0.1 <  $\gamma_o$  < 10; but  $\gamma_o$  < 2 for  $\omega$  = 50 and 100 rad/s) even though  $Wi = \dot{\gamma} \lambda = \dot{\gamma}$  0.265 s reached values of up to 28. In the flow curve measurements, the maximum Wi was 16 ( $\dot{\gamma}$  = 60 1/s) and the Cox-Merz rule could be applied. Gurnon and Wagner showed that the Cox-Merz rule fails for shear banding samples [10]. In absence of the stress plateau that is associated with shear banding and the validity of the Cox-Merz rule, we expect that our sample, which has a much smaller CTAB concentration (4.43 wt%) than the samples in the studies referenced above, does not shear band. Furthermore, shear banding is normally accompanied by a transient shear stress decay when the sample is sheared at rates in the shear thinning region. The time scale of this transient effect is usually at least two decades larger than the Maxwell relaxation time  $\lambda$  [43]. The absence of these long transients in our experiments further corroborates that the determined intrinsic nonlinearities are not influenced by shear banding.

#### 4 MODEL CALCULATIONS

#### 4.1 NONLINEAR WAVEFORMS

The numerical solution of the presented model gives an oscillatory stress signal  $\sigma(t)$  for an applied oscillatory strain input of  $\gamma(t) = \gamma_0 \sin \omega t$ . The relaxation modulus G linearly determines the stress scale of the results and was arbitrarily set to 10 Pa in all calculations. Exemplary results of the waveforms for G = 10 Pa,  $\lambda = 1 \text{ s}$ ,  $\omega = 1 \text{ rad/s}$ are shown in Figure 3 for four different strain amplitudes. Only the steady state solutions, after all transients have decayed, are shown. The elastic ( $\sigma$  versus  $\gamma$ , Figure 3 a) and viscous ( $\sigma$  versus  $\dot{\gamma}$  , Figure 3 b) Lissajous plots for a linear response at  $\gamma_o$  = 0.011 show an ellipse. In this case, De equals one and therefore the phase angle is exactly 45°, thus elastic and viscous behavior are balanced. At larger amplitudes, deviations from the elliptical form are visible. For  $\gamma_o$  = 1.33 in Figure 3a, the loop area exceeds the area of the loop at  $\gamma_o$  = 0.011. This means that the viscous contribution exceeds the elastic part (G'' > G'). The loop area equals the dissipated energy per unit volume in a cycle [4, 46, 47]. In the stress versus shear rate representation, the waveform for  $\gamma_o = 6$  is reminiscent of the typical, sigmoidal, nonlinear waveform of a polymer melt reported by Dealy et al. [48] and Tee and Dealy [49]. For  $\gamma_0$  = 23.7 pronounced nonlinear effects occur. At such high shear rates ( $\dot{\gamma}_{max} = \gamma_o \omega = 23.7 \text{ 1/s}$ ) the dashpot is

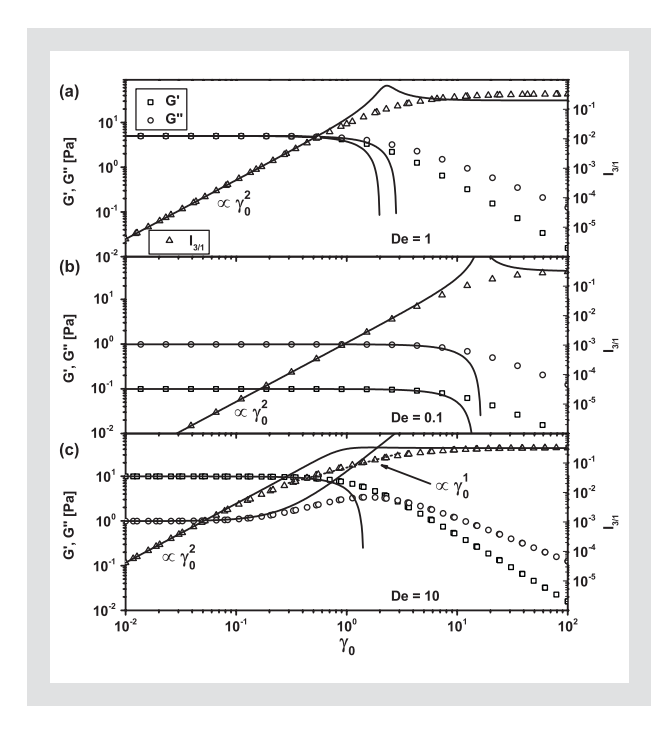


Figure 4: Symbols show G', G'' and  $I_{3/1}$  from a numerical solution of the model (Equation 12) using G=10 Pa and  $\omega=1$  rad/s. (a) limiting case:  $\lambda=1$  s and De=1, (b) viscous case:  $\lambda=0.1$  s and De=0.1, (c) elastic case:  $\lambda=10$  s and De=10. Solid lines are asymptotic analytical solutions (Equation 16) for the present model (Equation 12). They are exact for small enough deformation amplitudes only, see the appendix for a detailed derivation. The dashed line indicates a region where  $I_{3/1}$  is linear in  $\gamma_0$ . Note also the coinciding local maximum in G'' for De=10. Such a maximum is often observed in measurements of filled elastomers [55].

strongly shear thinning within the oscillation cycle (compare the shear rate dependent viscosity in Figure 2). This results in behavior reminiscent of an elastoplastic body [50]. An elastoplastic material shows elastic response as long as the stress is below the yield stress, a material specific model parameter. Above the yield stress, plastic flow is exhibited, that means the stress is independent of the shear rate. In the Lissajous representation, the waveform then resembles a parallelogram. In the elastoplastic model, the transition from elastic behavior to flow is discontinuous. At sufficiently large strain amplitudes, our model reproduces similar behavior, albeit in our case, the transition is smooth (see  $\gamma_o$  = 6.0 and  $\gamma_o$  = 23.7 in Figure 3a).

#### 4.2 FOURIER ANALYSIS

After exploring the waveforms qualitatively, quantitative measures for strain amplitude (or  $Wi = \omega \gamma_o \lambda$ ) dependent calculations are presented. Generally, for an arbitrary periodic stress signal, G' and G'' are computed by Equations 11 and 12 from the first harmonic stress amplitude  $\sigma_1$  and the phase angle  $\delta_1$ , which is referenced to the sinusoidal strain input. Since in the modified Maxwell model (Equation 10) the storage and loss moduli, G' and G'' become  $\gamma_o$  dependent, they can be described by Equation 6 only in the limit of sufficiently small  $\gamma_o$ .

$$G'(\gamma_o) = \frac{\sigma_i}{\gamma_o} \cos \delta \tag{11}$$

$$G''(\gamma_o) = \frac{\sigma_{\tau}}{\gamma_o} \sin \delta \tag{12}$$

Figure 4 displays the  $\gamma_o$  dependence of G', G', and  $I_{3/1}$  for G = 10 Pa at De = 0.1, 1, and 10. Variations in De can be achieved by altering the relaxation time or the angular frequency. Altering the relaxation time is equivalent to comparing different materials at the same frequency or, if time temperature superposition is valid, the same material at different temperatures and the same frequency. For the same viscoelastic material (constant  $\lambda$ ) changing the frequency leads to a change of the balance of viscous and elastic response. In Figure 4a for small  $\gamma_o$ , G' equals G'', which is consistent with Maxwellian behavior at De = 1. With increasing  $\gamma_o$ , the response becomes increasingly nonlinear: Both G' and G" start decreasing, but G' does so more drastically. A decreasing G' is primarily a signature of nonlinearity and in our model it is a consequence of the shear thinning dashpot, as the shear thinning leads to an overall decreasing stress amplitude. This decrease in G'cannot be interpreted as a weakening of the spring in the modified Maxwell model, since the spring is explicitly linear. This demonstrates how G' and G" lose their original interpretations in LAOS. Nevertheless they are still useful descriptors. The relative intensity of the third harmonic displays a power law behavior  $I_{3/1} \propto \gamma_o^2$  for sufficiently small  $\gamma_o$  (see for example  $\gamma_o$  < 0.4 in Figure 4a). This region is termed the intrinsic LAOS range [16, 17, 51] or MAOS (Medium Amplitude Oscillatory Shear [6]). Eventually,  $I_{3/1}$  levels off at value of 1/3, which is the maximum  $I_{3/1}$  when the waveform approaches a rectangle wave [52]. A rectangle waveform is produced by plastic behavior or in other words a shear thinning viscosity that follows a power law with an exponent of - 1 [46, 53]. Hence, at these high values of  $\gamma_o$  (and therefore high shear rate amplitudes), the effect of the incorporated spring is evident only at times around  $\gamma/\gamma_o = 1$  or -1 corresponding to  $\dot{\gamma}/\dot{\gamma}_o$  = 0 and the system displays plastic behavior for most of the cycle.

Along with the numerical results, asymptotic analytical solutions are plotted as solid lines in Figure 4. The differential equation (Equation 10) has been partially solved by assuming the nonlinear stress representation (Equation 13) according to Pearson an Rochefort [2] in order to obtain the first nonlinear terms that scale with  $\gamma_o{}^3$  or  $\dot{\gamma}_o{}^3$ , that is, the first terms that describe the deviation of G' and G'' from their plateau values. Furthermore an asymptotic expression for  $I_{3/1}$  (Equation 14) was derived, resembling the one in Giacomin et al. [54]. It is

expressed in terms of  $G'_{nm}$  and  $G''_{nm}$  coefficients from Equation 13, where n counts the order of the expansion in  $\gamma_o$  and m counts the harmonic number. The coefficients for n=1, 3 and m=1, 3 as well as the details of the solution can be found in the Appendix.

$$\sigma(t) = \sum_{n,odd} \sum_{m,odd}^{n} \gamma_{o}^{n} [G'_{nm}(\omega) sin(m\omega t) + G''_{nm}(\omega) cos(m\omega t)]$$
(13)

$$I_{3/1} = \frac{\sqrt{\left(G'_{33}\gamma_o^3 + ...\right)^2 + \left(G''_{33}\gamma_o^3 + ...\right)^2}}{\sqrt{\left(G'_{n}\gamma_o + G'_{31}\gamma_o^3 + ...\right)^2 + \left(G''_{n}\gamma_o G''_{31}\gamma_o^3 + ...\right)^2}}$$
(14)

The asymptotic solutions, shown as lines in Figure 4, confirm the numerical results for small deviations from the linear viscoelastic regime. However, already for  $\gamma_o > 1$  (for De = 1), the asymptotic predictions fall below the numerical results, because only the  $3^{\rm rd}$  order term in  $\gamma_o$  is included. Additionally, G' and G'' eventually become negative for increasing  $\gamma_o$ , which is unphysical and not shown in the log-log plots, and  $I_{3/1}$  exhibits an apparent maximum around  $\gamma_o = 2.3$ . The comparison to the numerical results shows that both effects are artifacts caused by the truncation. This demonstrates the limitation of the truncated expansion in Equation 13. To describe the numerical results in the full range that is plotted in Figure 4 many higher terms would be required in Equation 14.

After dealing with the special case of De = 1, the representative cases of predominantly viscous (De = o.1) and predominantly elastic behavior (De = 10) shown in Figures 4b and 4c are addressed. De was varied by choosing  $\lambda$  accordingly, while keeping  $\omega$  constant. For De = 0.1 (Figure 4b) in the linear regime, G'' is 10 times higher than G' and in the nonlinear regime both G' and G" decrease. When compared to the case of De = 1 the overall decrease of nonlinearity is evident in the decrease of the moduli occurring at larger  $\gamma_o$ . Similarly, although it has the same qualitative behavior as in Figure 4a,  $I_{3/1}$  shows smaller values, indicating that the transition from linear to nonlinear behavior occurs at larger  $\gamma_o$ . In the case of *De* = 10 (Figure 4c), the initial situation for small amplitudes is reversed, G' is 10 times higher than G", again recovering the results of the Maxwell model for the linear case. Interestingly, for De > 1 the model is able to predict an overshoot in G", followed by a cross-over of G' and G". These are common characteristics for yielding under LAOS that have been observed for dense colloidal suspensions, gels and foams [50, 56, 57]. In filled and vulcanized elastomers, this effect has also been observed and is known as the Payne effect [55, 58, 59]. Increased dissipation marked by the maximum in G" is commonly interpreted on the microscopic

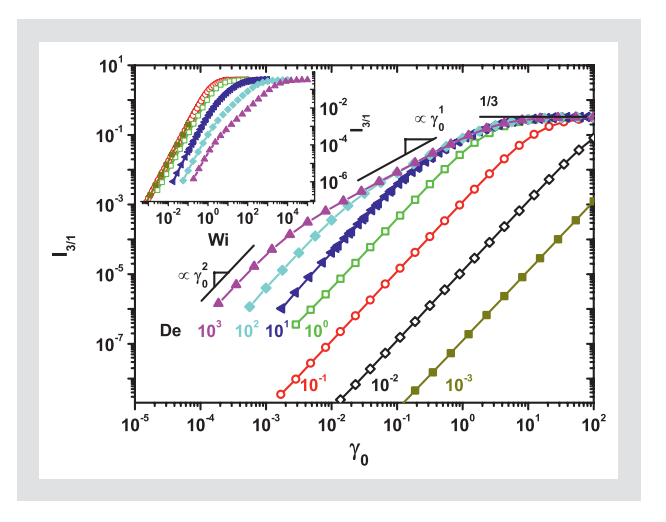


Figure 5:  $I_{3/1}$  for various  $De = \lambda \omega$  from numerical solutions of the model (Equation 12) using G = 10 Pa and  $\omega = 1$  rad/s/ Lines indicate scaling regions of  $I_{3/1} \propto \gamma_o^2$  and  $\gamma_o^1$ . Inset shows rescaled curves of  $I_{3/1}$  as a function of the Weissenberg number  $Wi = \dot{\gamma}_o \lambda = De \gamma_o$ .

scale as a signature for the break-up of network connections in these systems. Our results show that no specific network structure needs to be considered to produce this effect. In our model, predominantly elastic behavior (De > 1) in conjunction with shear thinning leads to the occurrence of the G" maximum. A close inspection of the numerically determined  $I_{3/1}$  reveals an intermediate scaling region (broken line in Figure 4c) where  $I_{3/1} \propto \gamma_o$  that also coincides with the increase in G".

Since by construction, nonlinearity in the model arises from the shear thinning dashpot, it seems surprising that we also find elastic nonlinearities in the LAOS response: By inspecting the sign of  $G'_{31}$  and  $G'_{33}$  of the asymptotic solution in the Appendix (Equations A.20 and A.22) or equivalently  $[e_1] = G'_{31}$  and  $[e_3] = -G'_{33}$  using the Chebishev polynomial basis [19], the elastic nonlinear contributions to the stress response can be classified as intercycle elastic softening and intracycle elastic strain softening. The reason for the occurrence of these elastic nonlinearities despite the linear spring is simply its serial coupling with the nonlinear dashpot. The resulting differential equation leads to waveforms that include signatures of viscous as well as elastic nonlinearity. For sufficiently high shear rates, the dashpot will behave nonlinearly producing a nonsinusoidal stress. Since the stress in both elements, spring and dashpot, is equal the spring is experiencing a nonsinusoidal stress as well. Due to its linear nature, its strain  $\gamma_s$  then must be nonsinusoidal. This shows that the interpretation of the signs of high harmonic moduli or of the intrinsic Chebishev coefficients do not provide information about the origin of the nonlinearity, (spring or dashpot) but only describe the resulting waveforms. Therefore, we refrain from a more detailed analysis using the Chebishev coefficient framework in the current work.

The calculations have been repeated for several other values of De and the results for  $I_{3/1}$  are shown in Figure 5. In all cases, an initial power law behavior with

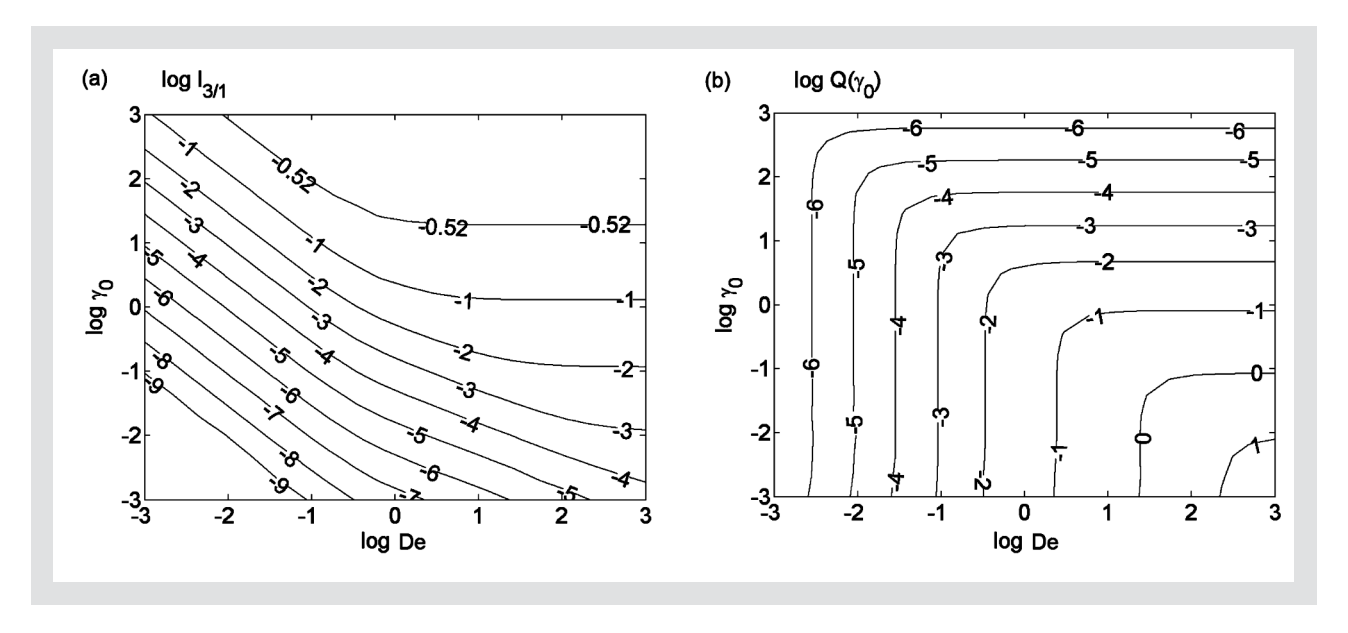


Figure 6: Contour plots of  $\log I_{3/1}(a)$  and  $\log Q(\gamma_o)$  (b), calculated for the present model (Equation 12) in the De -  $\gamma_o$  space, also known as Pipkin space [60]. For De < 1,  $I_{3/1}$  increases quadratically with  $\gamma_o$  in the plotted  $\gamma_o$  range, compare also to curves for De < 1 in Figure 5. In contrast, for De > 1, the distance between the contour lines increases corresponding to subquadratic increase of  $I_{3/1}$  with  $\gamma_o$ , compare to curves for De > 1 in Figure 5. The additional contour line at  $\log I_{3/1} = -0.52$  corresponds to  $I_{3/1} = 0.3$ .

 $I_{3/1} \propto \gamma_o^2$  can be observed for small  $\gamma_o$ , which is confirmed by the asymptotic solutions. Furthermore, for *De* > 1 the intermediate scaling region where  $I_{3/1}$  is linear in  $\gamma_o$  extends over a larger range of strain amplitudes for increasing *De*. Curves of  $I_{3/1}$  versus  $\gamma_o$  can be superimposed on a master curve for De < 0.1 when  $I_{3/1}$  is plotted versus  $Wi = \omega \gamma_o \lambda$  as shown in the inset of Figure 5. For De > 0.1, the superposition using Wi is not possible because the functional form of  $I_{3/1}$  changes when elastic contributions matter. The influence of the elastic spring also leads to different *De* scaling behavior of the  $I_{3/1}$  curves. An alternative way of displaying the nonlinearity measured by  $I_{3/1}$  is shown in Figure 6a. Here we plot  $\log I_{3/1}$ in the De –  $\gamma_o$  space. This representation is known as the Pipkin diagram [60]. For increasing  $\gamma_o$  and De,  $I_{3/1}$ peaks to its maximum of 1/3 in the large  $\gamma_o$  - high De corner of the plot. For De < 1,  $I_{3/1}$  increases quadratically with  $\gamma_o$  in the plotted  $\gamma_o$  range (compare also to curves for De < 1 in Figure 5). In contrast, for De > 1 the distance between the contour lines increases corresponding to a subquadratic increase of  $I_{3/1}$  with  $\gamma_o$  (compare to curves for De > 1 in Figure 5). In Figure 6b, the logarithm of  $Q(\gamma_o)$ , where  $Q(\gamma_o) = I_{3/1}/\gamma_o^2$  is plotted in the same coordinates. Reducing  $I_{3/1}$  to  $Q(\gamma_o)$ , eliminates the initial quadratic scaling for small  $\gamma_o$  and low De, evident in vertical contour lines of Figure 6b. Similar nonlinearity maps have been published for the Giesekus model [21] and for the Pom-Pom model [61].

#### 4.3 INTRINSIC NONLINEARITY Q0

From the regions where  $I_{3/1} \propto \gamma_o^2$  holds, the intrinsic nonlinearity  $Q_o(De) = \lim_{\gamma_o \to o} I_{3/1}/\gamma_o^2$  has been determined [16]. This material function depends on De (or  $\omega$  for a fixed relaxation time) only and can be interpreted as a measure of how early nonlinear behavior becomes im-

portant when the strain amplitude is increased. The Dedependence will always be implied for the rest of the paper and not written specifically as  $Q_o(De)$ . The strict definition of a linear viscoelastic regime is not possible in the intrinsic concept because  $I_{3/1}$  actually never equals o. But one can always assign a range where  $I_{3/1}$ is so small that the distortion plays an insignificant role for the overall mechanical behavior of a material. Such a limit could be set due to experimental limitation, for example, at  $I_{3/1} = 10^{-4}$ . This threshold seems reasonable since for all  $\gamma_o$  where  $I_{3/1}$  is smaller, the deviations of G'and G" from their respective small  $\gamma_o$  limits are vanishingly small (compare Figures 4a to 4c). With this definition of a 'practical' linear range in mind, larger  $Q_0$ , means narrower linear range, thus G' and G" deviate from their plateau values at smaller  $\gamma_o$ .

The dependence of  $Q_o$  on De is displayed in Figure 7. For  $De \ll 1$ ,  $Q_0$  increases quadratically with De, whereas for De >> 1 it is linear in De. The quadratic small De behavior is a typical signature of a shear thinning viscosity. At these conditions the dashpot is dominating the overall response and any viscosity function that can be  $represented\,as\,an\,ordered\,expansion\,in\,shear\,rate\,leads$ to  $Q_o \propto De^2$  in the limit of small De [62]. For De > 1 the influence of the linear spring becomes evident: Coupling the nonlinear dashpot to a linear spring reduces the increase of  $Q_o$  with *De* from quadratic to linear. The expectation that increasingly dominating elastic behavior, which is linear in the present model, would eventually lead to a reduction of overall nonlinearities for very large De is not met. This is due to only one relaxation time  $\lambda$  present in the model. An increasing  $\lambda$  =  $\eta/G$  at constant  $\omega$  corresponds to a more elastic material, but at the same time a larger value also shortens the linear range of the dashpot. Since the intrinsic nonlinearity  $Q_o$  reflects the first deviation of the dashpot from its zero shear viscosity, even for De > 1, the effect of the spring is to attenuate nonlinearity with increasing De.

Comparing to predictions of other available models, the present simple model predicts different behavior for the elastic region (Figure 7). For example, in the corotational Maxwell model (CRM) [54], Qo plateaus to a value of 1/24 ≈ 0.0416. Similarly, a constant value for  $Q_o$  is reached in the molecular stress function (MSF) model for large *De* (1/4( $\alpha - \beta$ /10)  $\approx$  0.0345, for  $\alpha = 5/21$ and  $\beta$  = 1 [13]). In the molecular model for a system of dilute rigid dumbbells [63], Qo also approaches a constant limit (3/28 ≈ 0.107) for large De. The Giesekus and the Pom-Pom model, in contrast predict a decrease in  $Q_o$  for De > 1. By comparing the large De limits of  $G'_{33}$ and  $G''_{33}$  in the different models, we determine the dominating contribution to  $Q_o$  (Equation 15) at large De. The denominator in Equation 15 asymptotes to the Maxwell parameter G for all presented models except the dumbbell model. For the two models that are time strain separable [12], the corotational Maxwell and the MSF model,  $G'_{33}$  exhibits a plateau in the  $De \rightarrow \infty$  limit and dominates over  $G_{33}^{"}$  leading to the constant value for  $Q_o$ . For time strain inseparable models (current model, Pom-Pom, and Giesekus model), the large De behavior of  $Q_o$  is dictated by  $G''_{33}$ . This is because the limit of  $G'_{33}$  is either constant while  $G''_{33}$  increases (see Equations A.22 and A.23 for the present model) or  $G'_{33}$  decreases stronger than the  $G''_{33}$  term (see Equations 4.6 and 4.7 in Hoyle et al. [11] for the Pom-Pom model and Equations A.51 and A.52 in the supporting information of Gurnon et al. [10] for the Giesekus model). Since the rigid dumbbell model of Bird et al. [63] has not been

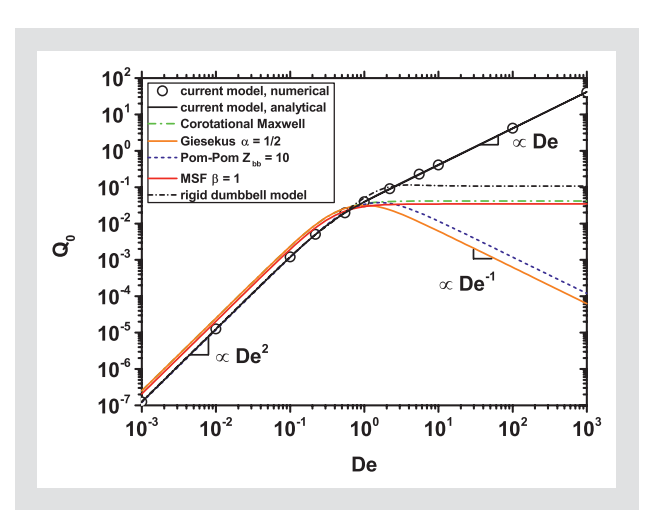


Figure 7: Intrinsic nonlinearity  $Q_o$  versus De for the current model, symbols are extracted from the small  $\gamma_o$  range where  $I_{3/1} \propto \gamma_o^2$  holds in Figure 5. Lines are analytical solutions for the various models collected in Table 1. In the Pom-Pom model  $Z_{bb}$  is the number of entanglements in the backbone.

written in integral form yet, it is unknown whether it is time strain separable. For this model,  $G''_{33} \propto De$  dominates over  $G'_{33} \propto De^o$  at large De, but since  $G''_{11} \propto De$ , this results in a plateau for  $Q_o$ . Which of the models performs best in describing  $Q_o$  of a simple viscoelastic fluid will be determined in the subsequently presented experimental section.

$$Q_{o} = \lim_{\gamma_{o} \to o} \frac{I_{3/7}}{\gamma_{o}^{2}} = \frac{\sqrt{G_{33}^{'2} + G_{33}^{"2}}}{\sqrt{G_{n}^{'2} + G_{n}^{"2}}}$$
(15)

Analytical expressions for  $Q_o$  from the different models are summarized in Table 1. Here we present the full analytical expressions, their small and large De limits, and simplified expressions that capture both limiting be-

Model	$Q_0$	$\lim_{De \to 0} Q_0$	$\lim_{De\to\infty} Q_0$	simplified $Q_0$ for small and large De	a	b	d
White-Metzner with $\eta(\dot{\gamma}) = \frac{\eta_0}{(1+\lambda^2 \dot{\gamma}^2)^{1/2}}$	$\frac{1}{8} \frac{\mathrm{De^2}}{(1+9\mathrm{De^2})^{1/2}}$	$\frac{1}{8}\mathrm{De}^2$	$\frac{1}{24}$ De	$\frac{1}{8} \frac{\mathrm{De^2}}{1+3\mathrm{De}}$	1/8	3	-1
Pom-Pom	$\frac{\mathrm{De^2(1-2.5Z_{bb}^{-1})}}{2\pi(1+\mathrm{De^2})^{1/2}(1+25\mathrm{De^2}Z_{bb}^{-2})^{1/2}(1+4\mathrm{De^2})^{1/2}}$	$\frac{1}{2\pi}(1 - 2.5Z_{bb}^{-1})\mathrm{De}^2$	$\frac{\frac{1-2.5Z_{bb}^{-1}}{2\pi\cdot 10Z_{bb}^{-1}}De^{-1}}{2\pi\cdot 10Z_{bb}^{-1}}$	$\frac{1}{2\pi} \frac{(1-2.5Z_{bb}^{-1})\mathrm{De}^2}{1+10Z_{bb}^{-1}\mathrm{De}^3}$	$\frac{1-2.5Z_{bb}^{-1}}{2\pi}$	$10Z_{bb}^{-1}$	1
Molecular stress function (MSF)	$\frac{3}{2}(\alpha - \beta/10) \frac{De^2}{(1+4De^2)^{1/2}(1+9De^2)^{1/2}}$	$\frac{3}{2}(\alpha - \beta/10)\mathrm{De}^2$	$\frac{1}{4}(\alpha - \beta/10)$	$\frac{3}{2}(\alpha - \beta/10)\frac{De^2}{1+6De^2}$	$\frac{3}{2}(\alpha-\beta/10)$	6	0
Corotational Maxwell (CRM)	$\frac{1}{4} \frac{De^2}{(1+4De^2)^{1/2} (1+9De^2)^{1/2}}$	$\frac{1}{4}\mathrm{De}^2$	$\frac{1}{24}$	$\frac{1}{4} \frac{\mathrm{De^2}}{1+6\mathrm{De^2}}$	$\frac{1}{4}$	6	0
Giesekus	$\frac{\alpha}{4} \frac{\text{De}^2(9\text{De}^2 + 4\alpha^2 - 12\alpha + 9)^{1/2}}{(1 + 4\text{De}^2)^{3/2}(1 + 9\text{De}^2)^{1/2}}$	$\frac{\alpha}{4}(4\alpha^2 - 12\alpha + 9)^{1/2}De^2$	$\frac{\alpha}{32} \mathrm{De}^{-1}$	$\frac{\alpha}{4} \frac{(4\alpha^2 - 12\alpha + 9)^{1/2} De^2}{1 + 8(4\alpha^2 - 12\alpha + 9)^{1/2} De^3}$	$\frac{\alpha(4\alpha^2-12\alpha+9)^{1/2}}{4}$	$8(4\alpha^2 - 12\alpha + 9)^{1/2}$	1
Rigid dumbbell	$\frac{9}{14}\sqrt{\frac{\left(1+De^2\right)\left(\begin{array}{c}625+9250De^2+26649De^4\\+214488De^6+11664De^8\\ \left(25+4De^2\right)\left(1+4De^2\right)^2\left(1+9De^2\right)^2\left(25+9De^2\right)^2}$	$\frac{9}{70}$ De <sup>2</sup>	$\frac{3}{28}$	$\frac{9}{70} \frac{De^2}{1 + \frac{6}{5}De^2}$	$\frac{9}{70}$	<u>6</u> 15	0
Experimental finding for linear monodisperse homopolymers [64]	$a rac{\mathrm{De^2}}{1 + b \mathrm{De^{2+d}}}$	$a\mathrm{De}^2$	$\frac{a}{b} \mathrm{De}^{-d}$	$a\frac{\mathrm{De^2}}{1+b\mathrm{De^2}+d}$	$0.32Z^{-1/2}$	$33.75Z^{-1}$	0.35

Table 1: Analytical expressions for  $Q_o$  for different viscoelastic models. The approximate expressions, which capture the small and large De behavior, in the third column have very similar functional forms. These expressions have been calculated using formulas for  $I_{3/1}$  from the following references: Pom-Pom [11], MSF [13], CRM [54], Giesekus [10]. In the Pom-Pom model,  $Z_{bb}$  is the number of entanglements that effectively leads to nonlinearities, for this only the backbone entanglements of a branched polymer are considered. It is defined as  $Z_{bb} = Z\Phi_{bb}$ , where Z is the number of entanglements per molecule and  $\Phi_{bb} = M_{bb}/M$  is the mass fraction of the backbone.

haviors for small and large De. The simplification introduces a deviation in comparison to the exact expressions of the second column, when De approaches one but also make the  $Q_o$  expressions much more tractable. The simplified versions all show a similar functional form that can be written as Equation 16.

$$Q_o = a \frac{De^2}{1 + bDe^{2+d}} \tag{16}$$

The coefficients are summarized in Table 1. This finding is especially intriguing since a similar expression has been proposed by Cziep et al. based on experimental data covering a range of linear, monodisperse homopolymer melts [64]. Therein, the authors provide experimental values for the parameters in Equation 16:  $a = 0.32Z^{-0.5}$ ,  $b = 33.75Z^{-1}$ , and d = 0.35, where a and bare dependent on the number of entanglements Z = $M_w/M_e$ . Recently, asymptotic solutions for LAOS flow have been presented for the corotational Maxwell, Giesekus, and MSF models and additionally for a model for rodlike polymers, an emulsion model as well as the Curtiss-Bird model [20]. The models have been compared based on intrinsic Chebishev coefficients [51]. Corotational Maxwell model predictions for the magnitudes of the four intrinsic Chebishev material functions for LAOS flow agreed for a poly(vinyl acetate)-Borax hydrogel. Similarly, we will test the quality of our model predictions with experimental data in the following section, although we will restrict ourselves to  $Q_o$  as a single nonlinear material function.

### 5 COMPARISON TO EXPERIMENTAL DATA OF A WORMLIKE MICELLES SOLUTION

To validate the model predictions, a solution of wormlike micelles based on the surfactant cetyltrimethylammonium bromide (CTAB) was chosen as a model system because it exhibits nearly single-relaxation time behavior at small strain amplitudes for a wide range of De [10, 38, 39]. The particular concentration was chosen such that the cross-over frequency of the material is in the middle of a frequency window suitable for the rheometer. Thus frequencies a decade lower and a decade higher than the crossover frequency could be conveniently tested. The results of frequency dependent experiments in the linear viscoelastic regime on a 0.15 Maqueous solution of CTAB in the presence of 1.5 M KBr are compared to the model predictions in Figure 8. The model parameters were determined as G = 68 Pa and  $\lambda$  = 0.265 s, by fitting the Maxwell expressions for G'and G" (Equation 6) to the data (Figure 8). Furthermore, the validity of the Cox-Merz rule can be confirmed for

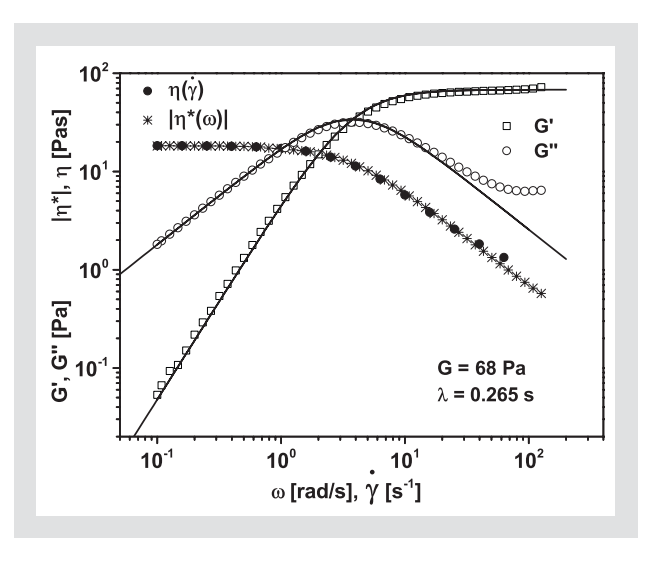


Figure 8: G' and G'' of a 0.15 M aqueous solution of CTAB in the presence of 1.5 M KBr at  $T=35^{\circ}$ C, measured at  $\gamma_{o}=0.1$ . Lines are fits of the Maxwell expressions for G' and G'' with G=68 Pa and  $\lambda=0.265$  s. Also shown is the validity of the Cox-Merz rule for this sample: The dependence of the absolute value of the complex viscosity  $|\eta^*|$  on  $\omega$  is the same as the dependence of the steady shear viscosity  $\eta$  on  $\dot{\gamma}$ .

the wormlike micelles solution in a frequency/shear rate range of almost three decades, where  $|\eta^*(\omega)| = \eta(\dot{\gamma})$ .

A quantitative comparison of model prediction and measured data for varying strain amplitudes is presented in Figure 9 in terms of G', G'', and  $I_{3/1}$ . In the linear viscoelastic regime, the agreement is, as expected very good. For increasing  $\gamma_{o}$ , the model captures the decrease in G' very well, but overestimates G", which decreases more steeply in the experiment. Intensities of  $I_{3/1}$  however, are underestimated by the model by approximately 30 % in the intrinsic range (0.5  $< \gamma_0 <$  2). The overall agreement for this frequency is comparable to results of [65], who modeled data of poly(ethylene oxide) and poly(acrylic acid) solutions with a multimode version of the tensorial Giesekus model. For frequencies exceeding the inverse of the relaxation time, our model predicts the Payne effect (a local maximum in G'' for increasing  $\gamma_o$ ) as shown in Figure 4. However, this rheological signature was not found for the CTAB sample investigated here. Instead, for the highest investigated shear rate amplitudes  $(\dot{\gamma}_o = 9.96 \text{ 1/s at } \omega = \text{10 rad/s and } \gamma_o = 9.96)$ , the strain amplitude dependent moduli G'and G"approached high shear rate plateaus after a shear thinning region.

As shown in Figure 9,  $I_{3/1} \propto \gamma_o^2$  for a certain range of  $\gamma_o$ , therefore the intrinsic nonlinearity  $Q_o$  can be determined. Frequency dependent measurements of  $Q_o$  of the CTAB sample are shown in Figure 10 along with the predictions of the current model. Repeated measurements with separate loadings show the reproducibility of the  $Q_o$  values (relative standard deviation 10–20%). The corotational Maxwell model which has the same model parameters, G and  $\lambda$ , is shown as well. In contrast to the current model, in the corotational Maxwell model, nonlinear behavior arises not from assuming a shear rate dependent viscosity, but is a con-

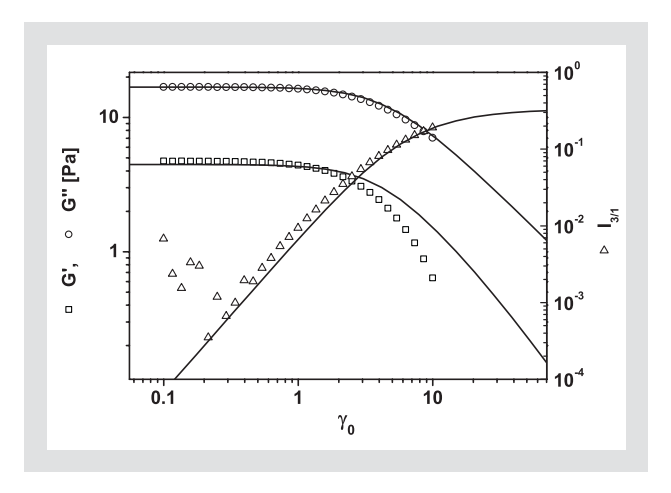


Figure 9: Strain amplitude dependent G', G'' and  $I_{3/1}$  for a 0.15 M aqueous solution of CTAB in the presence of 1.5 M KBr at T = 35°C and  $\omega = 1$  rad/s. Lines are model calculations (Equation 12) using G = 68 Pa,  $\lambda = 0.265$  s, and De = 0.265.

sequence of using a corotational derivative in the differential equation [9]. It is a three dimensional, that means second rank tensorial model, where the shear stress is coupled to normal stresses. The corotational derivative ensures frame invariance by rotating the coordinate frame with the fluid element, and defines the coupling of shear and normal stresses. This coupling allows one to predict nonlinear stress signals in LAOS flow. Although generally the modified Maxwell model predictions (Equation 10) fall below the measured nonlinearities for De < 1, the errors are not too grave, with the predicted values of Qo being 50 % below the measurements. Although the predictions of the 3D corotational Maxwell model are better, the presented simple modified Maxwell model shows reasonable capability of describing the data for De < 1. Its failure for De > 1 is not that surprising, as the assumption that the spring is always linear and only the dashpot is nonlinear, is unrealistic at conditions where elasticity dominates the material's mechanical properties. The power law exponent for the decrease in the large De range was found to be approximately - 0.16 for the specific sample investigated here. Fitting Equation 16 to the data gives a =0.2, b = 2.53, and d = 0.158.

Therefore, in comparison to measurements of linear, narrowly distributed polymer melts by Cziep et al. [64] where a d value of 0.35 was determined, in our wormlike micelles sample,  $Q_o$  decreases less steeply at large De. The differences in the large De behavior between the two systems are expected to be related to different relaxation mechanisms. On the microscopic level, the physics of wormlike micelles resemble macromolecules in that terminal relaxation occurs through reptation and at high frequencies segmental Rouse relaxation dominates [25, 66, 67]. Since the Rouse time scale is usually 2-3 decades shorter than the reptation time we think it unlikely to contribute to  $Q_o$  in the current measurements, which are limited in frequency to one decade above the inverse relaxation time. For polymer melts, deviations from Maxwellian behavior due to in-

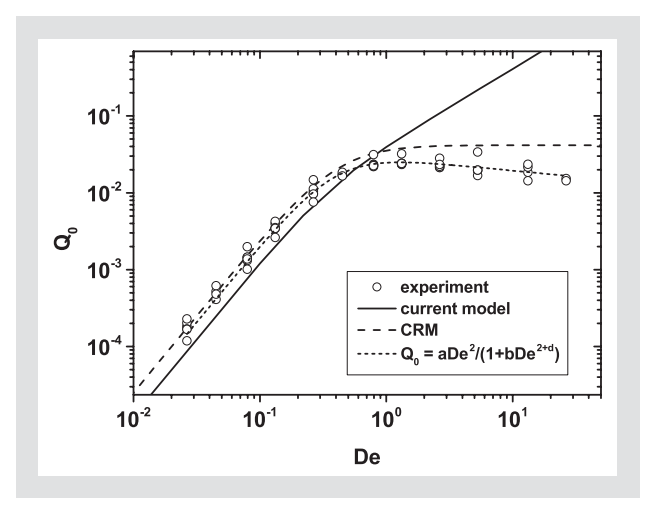


Figure 10:  $Q_o$  of a 0.15 M aqueous solution of CTAB in the presence of 1.5 M KBr at  $T=35\,^{\circ}$ C. Repeated measurements with separate loadings give an estimate of the reproducibility. Lines are predictions of the current model (Equation 12) and the corotational Maxwell model (CRM). Additionally, Equation 18 has been fitted to the data providing a=0.2, b=2.53, and d=0.158.

creased dissipation by processes such as contour fluctuations and constraint release [25], occur at comparatively low frequencies, close to the cross-over frequency, where G' = G''. These could be responsible for the universal scaling found for linear polymer melts [64]. In contrast to polymer melts, the breaking mechanism in wormlike micelles [39] allows a relaxation path distinct for these systems. The breaking time scale  $\lambda_{br}$  coincides with the inverse frequency of the minimum in G" from linear viscoelastic measurements [66]. For the investigated sample  $\lambda_{br}$  = 0.0107 s, is much shorter than  $\lambda_{rept}$  = 6.56 s which we calculate from  $\lambda$  = 0.265 s using the relationship  $\lambda = (\lambda_{br}\lambda_{rept})^{1/2}$  [68] for the fast breaking limit  $(\lambda_{br} \ll \lambda_{rept})$ . We speculate that the quantitatively different behavior in the intrinsic nonlinearity at large De is connected to the dominance of the breaking mechanism. To clarify this,  $Q_o(De)$  has to be determined for a range of WLM systems including linear, branched and network topologies and the universality of the large De scaling of  $Q_o(De)$  has to be investigated. Then, measurements on WLM samples in which breaking is not the dominating relaxation mechanism and the relaxation is not monoexponential are required, a task for future studies. Since none of the models shown in Figure 7 can predict the experimentally determined large *De* behavior quantitatively, the correct modeling of the elasticity dominated high frequency range remains a challenge.

### 6 CONCLUSIONS

A simple scalar model, capable of predicting nonlinearities for the large amplitude oscillatory shear experiment using only two parameters, a shear modulus and a relaxation time, has been presented. The model was obtained by replacing the linear dashpot in a Maxwell model by a nonlinear function, while the spring's mod-

ulus was held constant. The specific function for the nonlinear dashpot was chosen by applying the Cox-Merz rule  $|\eta^*(\omega)| = \eta(\dot{\gamma})$  to the expression of complex viscosity from the Maxwell model. The model is a scalar, special case of the White-Metzner model. Numerical solutions of the model have been calculated for a wide range of frequencies and strain amplitudes. The results analyzed by Fourier transform were presented in terms of the strain amplitude dependencies of the storage and loss moduli G' and G" the relative intensity of the third harmonic  $I_{3/1}$  and the intrinsic nonlinearity  $Q_o$ . Furthermore, an approximate analytical solution was provided in the form of a truncated power series in strain amplitude. Scaling laws for  $I_{3/1}$  known from previous experiments and predictions of other models were confirmed and the functional form of  $Q_o(De)$  was compared to predictions of other models (corotational Maxwell, Giesekus model, Pom-Pom, molecular stress function, dilute rigid dumbell model). Furthermore, predicted  $Q_o(De)$  behavior was compared to experimental data of a micellar solution of cetyltrimethylammonium bromide (CTAB). Agreement with the experiments is reasonably good considering the model's simplicity. For De < 1, the model underestimates values for  $Q_o$  by less than 50 %. Qualitative deviations occur for large Deborah numbers (or high angular frequencies), where elastic behavior is dominating.

#### **ACKNOWLEDGEMENTS**

Financial support by the German Research Foundation DFG (SPP 1273, WI 1911/17-1) is gratefully acknowledged by D. Merger. M. Abbasi thanks the Alexander von Humboldt foundation for funding. This research was also undertaken, in part, thanks to funding from the Canada Research Chairs program of the Government of Canada for the Natural Sciences and Engineering Research Council of Canada (NSERC) Tier 1 Canada Research Chair in Rheology. C. Saengow appreciates the support from the Royal Golden Jubilee Program of the Thailand Research Fund (Contract No. PHD/0116/2554).

### APPENDIX: ASYMPTOTIC ANALYTICAL SOLUTION

Here we derive an asymptotical solution for the present model, which is a specific case of the White-Metzner model. The White-Metzner constitutive equation can be written in differential form [24], where  $\dot{\gamma}_{(1)} = \nabla \mathbf{v} + (\nabla \mathbf{v})^T$  denotes the rate of strain tensor and  $\sigma_{(1)} = \sigma \partial/\partial t + \mathbf{v} \nabla \sigma - (\nabla \mathbf{v})^T \sigma - \sigma \nabla \mathbf{v}$  is the upper convected derivative of the stress tensor [29]:

$$\sigma + \frac{\eta(\dot{\gamma})}{G}\sigma_{(i)} = \eta(\dot{\gamma})\dot{\gamma}_{(i)} \tag{A.1}$$

The scalar equation for the shear stress component  $\sigma_{12} = \sigma$ , where the indices will be dropped for brevity is:

$$\sigma + \frac{\eta(\dot{\gamma})}{G}\dot{\sigma} = \eta(\dot{\gamma})\dot{\gamma} \tag{A.2}$$

The viscosity function in Equation A.2 will be replaced by the Carreau model:

$$\eta(\dot{\gamma}) = \frac{\eta_o}{\left(1 + \lambda^2 \dot{\gamma}^2\right)^{(1-c)/2}}$$
3)

where  $\lambda$  and  $\eta_o$  are relaxation time and zero shear viscosity, respectively. If c=0, then the Cox-Merz definition in Equation 8 is retrieved. In a LAOS experiment, the sample is subjected to a sinusoidal deformation  $\gamma(t)=\gamma_o\sin(\omega t)$  where the shear rate is:

$$\dot{\gamma} = \gamma_o \omega \cos(\omega t) \tag{A.4}$$

According to Pearson and Rochefort [2], the nonlinear shear stress response under LAOS flow can be expanded as a  $n^{\text{th}}$  order power series in  $\gamma_o$  of a  $m^{\text{th}}$  order Fourier series in  $\omega$  with m counting the harmonics as given by:

$$\sigma(t) = \sum_{n,odd} \sum_{m,odd}^{n} \gamma_{o}^{n} [G'_{nm}(\omega) sin(m\omega t) + G''_{nm}(\omega) cos(m\omega t)]$$
(A.5)

Writing the first terms in  $\gamma_o$  ( $n \le 3$ ) and including the third harmonic ( $m \le 3$ ) explicitly gives:

$$\sigma(t) = \gamma_{o} \left[ G'_{n}(\omega) sin(\omega t) + G''_{n}(\omega) cos(\omega t) \right]$$

$$+ \gamma_{o}^{3} \left[ G'_{3}(\omega) sin(\omega t) + G''_{3}(\omega) cos(\omega t) + \right] + O(\gamma_{o}^{5})$$

$$\left[ G'_{3}(\omega) sin(3\omega t) + G''_{3}(\omega) cos(3\omega t) \right] + O(\gamma_{o}^{5})$$
(A.6)

$$\sigma(t) = \gamma_o \omega \left[ G_n(\omega) \cos(\omega t) - G_n(\omega) \sin(\omega t) \right]$$

$$+ \gamma_o^3 \omega \left[ G'_{31}(\omega) \cos(\omega t) - G''_{31}(\omega) \sin(\omega t) \right] + O(\gamma_o^5)$$

$$+ 3G'_{33}(\omega) \cos(3\omega t) - 3G''_{33}(\omega) \sin(3\omega t) \right] + O(\gamma_o^5)$$
(A.7)

Equation A.3 shows that the viscosity is a nonlinear function of shear rate, where a Taylor expansion for the nonlinear part of the Equation A.3 leads to:

$$\left(1 + \lambda^2 \dot{\gamma}^2\right)^{(1-c)/2} \approx 1 + \frac{1-c}{2} \lambda^2 \dot{\gamma}^2 + O(\dot{\gamma}_o^4) \tag{A.8}$$

Combination of Equations A.2 and A.8 results in:

$$\frac{G}{\eta_o} \left( 1 + \frac{1 - c}{2} \lambda^2 \dot{\gamma}^2 O(\dot{\gamma}_o^4) \right) \sigma + \dot{\sigma} - G \dot{\gamma} = 0$$
(A.9)

Equations A.4, A.6, and A.7 are inserted into Equation A.9 and considering  $\lambda = \eta_o/G$  and introducing the Deborah number  $De = \lambda \omega$  gives:

$$\left[ 1 + \frac{1-C}{2} \gamma_o^2 D e^2 \cos^2(\omega t) \right] \left[ \gamma_o \left[ G'_{1,s} \sin(\omega t) + G''_{1,s} \cos(\omega t) \right] \\ + \gamma_o \left[ G'_{1,s} \sin(\omega t) + G''_{1,s} \cos(\omega t) + G'_{1,s} \sin(3\omega t) + G''_{1,s} \cos(3\omega t) \right] \right]$$
 
$$+ \gamma_o D e \left[ G'_{1,s} \cos(\omega t) - G''_{1,s} \sin(\omega t) \right]$$
 
$$+ \gamma_o^3 D e \left[ G'_{1,s} \cos(\omega t) - G''_{1,s} \sin(\omega t) + 3G'_{1,s} \cos(3\omega t) - 3G''_{1,s} \sin(3\omega t) \right]$$
 
$$- G \gamma_o D e \cos(\omega t) + O(\gamma_o^4) = o$$
 
$$\left( A.10 \right)$$

Rearrangement of Equation A.10, collecting factors of  $\cos(\omega t)$ ,  $\sin(\omega t)$ ,  $\cos(3\omega t)$ , and  $\sin(3\omega t)$  up to the third power of  $\gamma_o$  results in:

$$\begin{split} &\left[-G\gamma_{o}De + \gamma_{o}DeG'_{n} + \gamma_{o}G''_{n} + \frac{3(1-c)}{8}\gamma_{o}^{3}De^{2}G''_{n} + \gamma_{o}^{3}DeG'_{3i} + \gamma_{o}^{3}G''_{3i}\right] cos(\omega t) + \\ &\left[\gamma_{o}G'_{n} - \gamma_{o}DeG''_{n} + \frac{(1-c)}{8}\gamma_{o}^{3}De^{2}G'_{n} + \gamma_{o}^{3}G'_{3i} + \gamma_{o}^{3}DeG''_{3i}\right] sin(\omega t) + \\ &\left[\frac{(1-c)}{8}\gamma_{o}^{3}De^{2}G''_{n} + 3\gamma_{o}^{3}De^{2}G'_{3i} + \gamma_{o}^{3}G''_{3j}\right] cos(3\omega t) + \\ &\left[\frac{(1-c)}{8}\gamma_{o}^{3}De^{2}G'_{n} + \gamma_{o}^{3}G'_{3i} - 3\gamma_{o}^{3}DeG''_{3i}\right] sin(3\omega t) + O(\gamma_{o}^{5}) = o \end{split}$$

In the linear viscoelastic regime terms higher than the first, i.e.  $O(\gamma_o^3)$  can be ignored. Therefore, the storage and loss modulus  $G'_n$  and  $G'_n$  can be obtained from Equation A.11, when the prefactors of the  $\cos(\omega t)$  and  $\sin(\omega t)$  terms are set to be zero:

$$-G\omega\lambda + \omega\lambda G'_{n} + G''_{n} = o \tag{A.12}$$

$$G'_{n} - \omega \lambda G''_{n} = 0$$
 (A.13)

Solving Equations A.12 and A.13 results in:

$$G'_{n} = G \frac{De^{2}}{1 + De^{2}}$$
 (A.14)

$$G''_{n} = G \frac{De}{1 + De^{2}} \tag{A.15}$$

This shows that the model predicts the Maxwell model behavior in the limit of linear viscoelasticity, as it should. Using Equations A.14 and A.15 in Equation A.11 and equating the prefactors of  $\cos(\omega t)$ ,  $\sin(\omega t)$ ,  $\cos(3\omega t)$ , and  $\sin(3\omega t)$  to zero gives four equations for the nonlinear terms  $G'_{3n}$ ,  $G''_{3n}$ ,  $G''_{3n}$ , and  $G''_{33}$ :

$$\frac{3(1-c)}{8}G\frac{De^{3}}{1+De^{2}}+DeG'_{31}+G''_{31}=0$$
(A.16)

$$\frac{(1-c)}{8}G\frac{De^4}{1+De^2} + G'_{31} - DeG''_{31} = 0$$
(A.17)

$$\frac{(1-c)}{8}G\frac{De^3}{1+De^2} + 3DeG'_{33} + G''_{33} = 0$$
(A.18)

$$\frac{(1-c)}{8}G\frac{De^4}{1+De^2} + G'_{33} - 3DeG''_{33} = 0$$
(A.19)

Solving Equations A.16 to A.19 the yields higher order moduli:

$$G'_{31} = -\frac{(1-c)}{2}G\frac{De^4}{(1+De^2)^2}$$
 (A.20)

$$G''_{31} = \frac{(1-c)}{8}G\frac{De^{3}(De^{2}-3)}{(1+De^{2})^{2}}$$
(A.21)

$$G'_{33} = -\frac{(1-c)}{2}G\frac{De^4}{(1+De^2)(1+9De^2)}$$
(A.22)

$$G''_{33} = \frac{(1-c)}{8}G\frac{De^{3}(3De^{2}-1)}{(1+De^{2})(1+9De^{2})}$$
(A.23)

The relative intensity of third harmonic  $I_{3/1}$  and the intrinsic nonlinearity  $Q_o$  [16] can then be calculated as:

$$\frac{I_{3}}{I_{1}} = \frac{\sqrt{\left(G'_{33}\gamma_{o}^{3} + G'_{53}\gamma_{o}^{5} + ...\right)^{2} + \left(G''_{33}\gamma_{o}^{3} + G''_{53}\gamma_{o}^{5} + ...\right)^{2}}}{\sqrt{\left(G'_{n}\gamma_{o} + G''_{31}\gamma_{o}^{3} + ...\right)^{2} + \left(G''_{n}\gamma_{o} + G''_{31}\gamma_{o}^{3} + ...\right)^{2}}}$$

$$= \frac{\sqrt{G'_{33}^{2} + G''_{33}^{2} + O(\gamma_{o}^{2})...}}{\sqrt{G'_{n}^{2} + G''_{n}^{2} + O(\gamma_{o}^{2})...}} \times \frac{\gamma_{o}^{3}}{\gamma_{o}} = Q(\omega, \gamma_{o})\gamma_{o}^{2}$$
(A.24)

Therefore:

$$Q_{o} = \lim_{\gamma_{o} \to o} I_{3/1} / \gamma_{o}^{2} = \frac{1}{8} \frac{De^{2}}{\left(1 + gDe^{2}\right)^{1/2}}$$
(A.25)

In the asymptotic limit for small *De*, Equation A.25 reduces to:

$$\lim_{De\to o} Q_o = \frac{(1-c)}{8} De^2 \tag{A.26}$$

Equation A.26 shows that the De dependence of  $Q_o$  is quadratic for small De, whereas the asymptotic limit for large De is a linear function of De:

$$\lim_{De\to o} Q_o = \frac{(1-c)}{24} De$$
 (A.27)

Combining Equations A.26 and A.27 results in Equation A.28, which captures both limiting behaviors.

$$Q_{o,a} = \frac{(1-c)}{8} \frac{De^{2}}{(1+3De)}$$
 (A.28)

The approximate function  $Q_o$ , a has then the form of Equation 16 but is inexact in comparison to Equation A.26 around De = 1.

#### REFERENCES

- [1] Dodge JS, Krieger IM: Oscillatory shear of nonlinear fluids I. Preliminary investigation, Trans. Soc. Rheol. 15 (1971) 589 601.
- [2] Pearson DS, <u>Rochefort WE: Behavior of concentrated polystyrene solutions in largeamplitude oscillating shear fields</u>, J. Polym. Sci., Part B: Polym. Phys. 20 (1982) 83 98.
- [3] Giacomin AJ, Jeyaseelan RS: A constitutive theory for polyolefins in large amplitude oscillatory shear, Polym. Eng. Sci. 35 (1995) 768–777.
- [4] Giacomin AJ, Dealy JM: Using large-amplitude oscillatory shear, in Rheological Measurement, Kluwer Academic Publishers, Dordrecht, Netherlands (1998).
- [5] Wilhelm M: <u>Fourier-transform</u> rheology, Macromol. Mater. Eng. 287 (2002) 83–105.
- [6] Hyun K, Wilhelm M, Klein CO, Cho KS, Nam JG, Ahn KH, Lee SJ, Ewoldt RH, McKinley GH: A review of nonlinear oscillatory shear tests: Analysis and application of large amplitude oscillatory shear (LAOS), Prog. Polym. Sci. 36 (2011) 1697–1753.
- [7] Dealy JM: Weissenberg and Deborah numbers Their definition and use, Rheol. Bull. 79 (2010) 14-18.
- [8] Blackwell BC, Ewoldt RH: A simple thixotropic-viscoelastic constitutive model produces unique signatures in large-amplitude oscillatory shear (LAOS), J. Non-Newton. Fluid. 208–209 (2014) 27–41.
- [9] Giacomin AJ, Bird RB, Johnson LM, Mix AW: Large-amplitude oscillatory shear flow from the corotational Maxwell model, J. Non-Newton. Fluid. Mech. 166 (2011) 1081–1099.
- [10] Gurnon KA, Wagner NJ: Large amplitude oscillatory shear (LAOS) measurements to obtain constitutive equation model parameters: Giesekus model of banding and nonbanding wormlike micelles, J. Rheol. 56 (2012) 333-351.
- [11] Hoyle DM, Auhl D, Harlen OG, Barroso VC, Wilhelm M, McLeish TCB: Large amplitude oscillatory shear and Fourier transform rheology analysis of branched polymer melts, J. Rheol. 58 (2014) 969–997.

- [12] Wagner M, Rolón-Garrido VH, Hyun K, Wilhelm M: Analysis of medium amplitude oscillatory shear data of entangled linear and model comb polymers, J. Rheol. 55 (2011) 495–516.
- [13] Abbasi M, Ebrahimi NG, Wilhelm M: Investigation of the rheological behavior of industrial tubular and autoclave LDPEs under SAOS, LAOS, transient shear, and elongational flows compared with predictions from the MSF theory, J. Rheol. 57 (2013) 1693–1714.
- [14] Saengow C, Giacomin AJ, Kolitawong C: Exact Analytical solution for large-amplitude oscillatory shear flow, Macromol. Theory Simul. 24 (2015) 352–392.
- [15] Boisly M, Kästner M, Brummund J, Ulbricht V: Large amplitude oscillatory shear of the Prandtl element analysed by Fourier transform rheology, Appl. Rheol. 24 (2014) 35478.
- [16] Hyun K, Wilhelm M: Establishing a new mechanical nonlinear coefficient Q from FT Rheology: First investigation of entangled linear and comb polymer model systems, Macromolecules 42 (2009) 411–422.
- [17] Reinheimer K, Grosso M, Hetzel F, Kübel J, Wilhelm M: Fourier transform rheology as an innovative morphological characterization technique for the emulsion volume average radius and its distribution, J. Colloid Interface Sci. 380 (2012) 201–212.
- [18] Giacomin AJ, Bird RB, Johnson LM, Mix AW: Corrigenda: Large-amplitude oscillatory shear flow from the corotational maxwell model [J. Non-Newtonian Fluid Mech. 166, 1081-1099 (2011)], J. Non-Newton. Fluid. Mech. 187-188 (2012) 48-48.
- [19] Ewoldt RH: <u>Defining nonlinear rheological material</u> functions for oscillatory shear, J. Rheol. 57 (2013) 177–195.
- [20] Bharadwaj NA, Ewoldt RH: Constitutive model fingerprints in medium-amplitude oscillatory shear, J. Rheol. 59 (2015) 557–592.
- [21] Ewoldt RH, Hosoi AE, McKinley GH: New measures for characterizing nonlinear viscoelasticity in large amplitude oscillatory shear, J. Rheol. 52 (2008) 1427–1458.
- [22] Rogers SA, Erwin BM, Vlassopoulos D, Cloitre M: A sequence of physical processes determined and quantified in LAOS: application to a yield stress fluid, J. Rheol. 55 (2011) 435–458.
- [23] Giacomin AJ: A sliding plate melt rheometer incorporating a shear stress transducer, Ph.D. thesis, McGill University (1987).
- [24] White JL, Metzner AB: Development of constitutive equations for polymeric melts and solutions, J. Appl. Polym. Sci. 7 (1963) 1867–1889.
- [25] Dealy JM, Larson RG: Structure and rheology of molten polymers, Hanser, Munich (2006).
- [26] Morrison FA: Understanding rheology, Oxford University Press, New York (2001).
- [27] Malkin A: Non-Newtonian viscosity in steady-state shear flows, J. Non-Newton. Fluid. 192 (2013) 48 65.
- [28] Zacharatos A, Kontou E: Nonlinear viscoelastic modeling of soft polymers, J. Appl. Polym. Sci. 132 (2015) 42141.
- [29] Bird RB, Armstrong RC, Hassager O: Dynamics of polymeric liquids, John Wiley & Sons, New York (1987).
- [30] Monsia MD: A simplified nonlinear generalized maxwell model for predicting the time dependent behavior of viscoelastic materials, World J. Mech. 1 (2011) 158–167.

- [31] Herrchen M, Öttinger HC: A detailed comparison of various FENE dumbbell models, J. Non-Newton. Fluid. 68 (1997) 17–42.
- [32] Kökuti Z, Völker-Pop L, Brandstätter M, Kokavecz J, Ailer P, Palkovics L, Szabó G, Czirák A: Exploring the nonlinear viscoelasticity of a high viscosity silicone oil with LAOS, Appl. Rheol. 26 (2016) 14289.
- [33] Yasuda K, Armstrong R, Cohen R: Shear flow properties of concentrated solutions of linear and star branched polystyrenes, Rheol. Acta 20 (1981) 163–178.
- [34] Cross MM: Polymer systems: Deformation and flow, Macmillan (1968).
- [35] Cox WP, Merz EH: <u>Correlation of dynamic and steady</u> flow viscosities, J. Polym. Sci. 28 (1958) 619 622.
- [36] Snijkers F, Vlassopoulos D: Appraisal of the Cox-Merz rule for well-characterized entangled linear and branched polymers, Rheol. Acta 53 (2014) 935 946.
- [37] Merger D: Large amplitude oscillatory shear investigations of colloidal systems: experiments and constitutive model predictions, Ph.D. thesis, Karlsruhe Institute of Technology (2015).
- [38] Khatory A, Lequeux F, Kern F, Candau SJ: Linear and nonlinear viscoelasticity of semidilute solutions of wormlike micelles at high salt content, Langmuir 9 (1993) 1456–1464.
- [39] Rehage H, Hoffmann H: <u>Viscoelastic surfactant solutions</u>: Model systems for rheological research, Mol. Phys. 74 (1991) 933 973.
- [40] Mair RW, Callaghan PT: Observation of shear banding in worm-like micelles by NMR velocity imaging, Europhys. Lett. 36 (1996) 719–724.
- [41] Britton MM, Callaghan PT: Two-phase shear band structures at uniform stress, Phys. Rev. Lett. 78 (1997) 4930 4933.
- [42] Salmon JB, Colin A, Manneville S: Velocity profiles in shear-banding wormlike micelles, Phys. Rev. Lett. 90 (2003) 228303.
- [43] Berret JF: Rheology of wormlike micelles: Equilibrium properties and shear banding transitions, in Molecular gels, Springer (2006).
- [44] Helgeson ME, Reichert MD, Hu YT, Wagner NJ: Relating shear banding, structure, and phase behavior in worm-like micellar solutions, Soft Matter 5 (2009) 3858–3869.
- [45] Helgeson ME, Vasquez PA, Wagner NJ: Rheology and spatially resolved structure of cetyltrimethylammonium bromide wormlike micelles through the shear banding transition, J. Rheol. 53 (2009) 727 756.
- [46] Ewoldt RH, Winter P, Maxey J, McKinley GH: Large amplitude oscillatory shear of pseudoplastic and elastoviscoplastic materials, Rheol. Acta 49 (2010) 191–212.
- [47] Giacomin AJ, Bird RB, Aumnate C, Mertz AM, Schmalzer AM, Mix AW: Viscous heating in large-amplitude oscillatory shear flow, Phys. Fluids 24 (2012) 103101.
- [48] Dealy JM, Petersen JF, Tee, TT: A concentric-cylinder rheomter for polymer melts, Rheol. Acta 12 (1973) 550-558.
- [49] Tee TT, Dealy JM: Nonlinear viscoelasticity of polymer melts, Trans. Soc. Rheol. 19 (1975) 595 615.
- [50] Rouyer F, Cohen-Addad S, Höhler R, Sollich P, Fielding SM: The large amplitude oscillatory strain response of aqueous foam: Strain localization and full stress Fourier spectrum, Eur. Phys. J. E 27 (2008) 309 – 321.
- [51] Ewoldt RH, Bharadwaj NA: Low-dimensional intrinsic

- material functions for nonlinear viscoelasticity, Rheol. Acta 52 (2013) 201–219.
- [52] Klein C, Spiess HW, Calin A, Balan C, Wilhelm M: Separation of the nonlinear oscillatory response into a superposition of linear, strain hardening, strain softening, and wall slip response, Macromolecules 40 (2007) 4250 4259.
- [53] Wilhelm M, Maring D, Spiess HW: Fourier-transform rheology, Rheol. Acta 37 (1998) 399 405.
- [54] Giacomin AJ, Gilbert PH, Merger D, Wilhelm M: Largeamplitude oscillatory shear: comparing parallel-disk with cone-plate flow, Rheol. Acta 54 (2015) 263–285.
- [55] Leblanc JL: Filled Polymers Science and industrial applications, CRC Press, Boca Raton (2010).
- [56] Brader JM, Siebenbürger M, Ballauff M, Reinheimer K, Wilhelm M, Frey SJ, Weysser F, Fuchs M: Nonlinear response of dense colloidal suspensions under oscillatory shear: Mode-coupling theory and Fourier transform rheology experiments, Phys. Rev. E 82 (2010) 061401.
- [57] Kim J, Merger D, Wilhelm M, Helgeson ME: Microstructure and nonlinear signatures of yielding in a heterogeneous colloidal gel under large amplitude oscillatory shear, J. Rheol. 58 (2014) 1359 1390.
- [58] Payne AR: The dynamic properties of carbon black-loaded natural rubber vulcanizates, J. Appl. Polym. Sci. VI (1962) 57–63.
- [59] Allegra G, Raos G, Vacatello M: Theories and simulations of polymer-based nanocomposites: From chain statistics to reinforcement, Prog. Polym. Sci. 33 (2008) 683-731.
- [60] Pipkin AC: Lectures in viscoelastic theory, Springer (1972).
- [61] Hyun K, Kim W, Park SJ, Wilhelm M: Numerical simulation results of the nonlinear coefficient Q from FT-Rheology using a single mode pom-pom model, J. Rheol. 57 (2013) 1–25.
- [62] Bharadwaj NA, Ewoldt RH: The general low-frequency prediction for asymptotically nonlinear material functions in oscillatory shear, J. Rheol. 58 (2014) 891–910.
- [63] Bird RB, Giacomin AJ, Schmalzer AM, Aumnate C: Dilute rigid dumbbell suspensions in large-amplitude oscillatory shear flow: Shear stress response, J. Chem. Phys. 140 (2014) 074904.
- [64] Cziep MA, Abbasi M, Heck M, Wilhelm M: Effect of molecular weight, polydispersity and monomer of linear homopolymer melts on the intrinsic mechanical nonlinearity  ${}^3Q_o(\omega)$  in MAOS, Macromolecules 49 (2016) 3566–3579.
- [65] Nam JG, Ahn KH, Lee, SJ, Hyun K: First normal stress difference of entangled polymer solutions in large amplitude oscillatory shear flow, J. Rheol. 54 (2010) 1243 1266.
- [66] Yesilata B, Clasen, C, McKinley GH: Nonlinear shear and extensional flow dynamics of wormlike surfactant solutions, J. Non.-Newtonian Fluid Mech. 133 (2006) 73–90.
- [67] Buchanan M, Atakhorrami,M, Palierne JF, MacKintosh FC, Schmidt CF: High-frequency microrheology of worm-like micelles, Phys. Rev. E 72 (2005) 011504.
- [68] Cates ME, Candau SJ: Statics and dynamics of worm-like surfactant micelles, J. Phys.: Condens. Matter 2 (1990) 6869–6892.

